Materials Research Bulletin 48 (2013) 25–29

Contents lists available at SciVerse ScienceDirect

Materials Research Bulletin

journal homepage: www.elsevier.com/locate/matresbu

Two-dimensional ZnO nanoflakes coated mesh for the separation of water and oil

Hong Li [a,b], Maojun Zheng [a,*], Li Ma [c], Changqing Zhu [a], Sheng Lu [c]

[a] Department of Physics, Shanghai Jiao Tong University, Shanghai 200240, PR China
[b] Department of Physics and Electronic Information, Huaibei Normal University, Huaibei 235000, PR China
[c] School of Chemistry & Chemical Technology, Shanghai Jiao Tong University, Shanghai 200240, PR China

ARTICLE INFO

Article history:
Received 11 June 2012
Received in revised form 7 September 2012
Accepted 29 September 2012
Available online 8 October 2012

Keywords:
A. Interfaces
A. Nanostructures
B. Sputtering
D. Surface properties

ABSTRACT

Through the low-temperature hydrothermal route, one kind of two-dimensional (2D) ZnO nanoflakes was grown on the stainless steel mesh coated by Al. After being modified by stearic acid (SA), the coated mesh was found to be superhydrophobic and superoleophilic simultaneously, and the water contact angle can reach to 156.3 ± 2.1°. It could separate a variety of water and oil mixture. The separation efficiency was up to 95%. It was found that the oil with larger surface tension can be easier to penetrate the coated mesh, and then the separate efficiency increased. Besides, a detailed investigation showed that the special hierarchical micro/nanostructures and appropriate size of the mesh played an important role in obtaining the superhydrophobicity and superoleophilicity. The coated mesh might be practically employed in oil pollution.

1. Introduction

In modern society, there is a growing need for the effective separation of water and oil because of the increasing oil pollution [1–3]. However, the separation of water and oil is a huge challenge, due to low separation efficiency, high operation costs and complex separation instrument. In order to overcome these difficulties, materials with both superhydrophobic and superoleophilic properties have received considerable attention in recent years [4]. Wettability is an important characteristic of solid surface, which can be controlled by the surface energy and geometric structure [5–7]. It was reported that the hydrophobicity and oleophilicity of a surface could be amplified by increasing the roughness of low surface energy materials [8–15], because the contact area between the surface and the water droplet was minimized by trapped air. On the basis of this principle, many methods have been developed to create such materials. For example, Jiang et al. fabricated a mesh for water and oil separation via coating copper mesh with polytetrafluoroethylene (PTFE) [4]. Tu et al. modified a stainless steel mesh with polystyrene solution for water and oil separation [16]. Pan et al. fabricated a superhydrophobic and superoleophilic copper filter by immersing mesh in aqueous solution of NaOH and $K_2S_2O_8$ and subsequently modifying it with n-dodecanethiol [17].

In this paper, we presented the growth of 2D ZnO nanoflakes on the stainless steel mesh through low-temperature hydrothermal route. After being modified by stearic acid, the coated mesh could separate oil from water and oil mixture selectively and effectively without any extra power. Its maximum of separation efficiency was above 95%. Besides, it was found that the separation efficiency mainly depended on the surface tension of oil, and the oil with larger surface tension could be easier to penetrate the mesh. The 2D ZnO nanoflakes coated mesh with special hierarchical micro/nanostructures may be practically applied to the separation of water and oil.

2. Experimental

A stainless steel mesh with an average pore diameter of approximately 75 μm was used as the substrate. The mesh was sequentially cleaned with detergent, deionized water, ethanol, acetone, and deionized water before being dried at 60 °C for 20 min. The Al film layers were deposited onto the mesh by direct current (DC) magnetron sputtering. The distance between the target and the substrate was about 60 mm. Before deposition, the chamber was pumped down to a base pressure of 1.5×10^{-5} Torr. During the growth of Al film, argon gas with a flow rate of 30 sccm was fed into the chamber. The applied DC power, working pressure and the deposition time were 50 W, 22 mTorr and 40 min, respectively. The thickness of the aluminum film on the stainless steel mesh is about 500 nm. After deposition, the mesh was dipped in a capped Pyrex glass bottle filled with 16 mM zinc nitrate hydrate ($Zn(NO_3)_2{\cdot}6H_2O$) and 16 mM hexamethylenetetramine (HMT, $C_6H_{12}N_4$) for growing 2D ZnO nanoflakes [18]. The Pyrex glass bottle was sealed and maintained at 90 °C for 2 h in a regular

* Corresponding author. Tel.: +86 21 34202791; fax: +86 21 34202791.
E-mail address: mjzheng@sjtu.edu.cn (M. Zheng).

0025-5408/$ – see front matter © 2012 Elsevier Ltd. All rights reserved.
http://dx.doi.org/10.1016/j.materresbull.2012.09.062

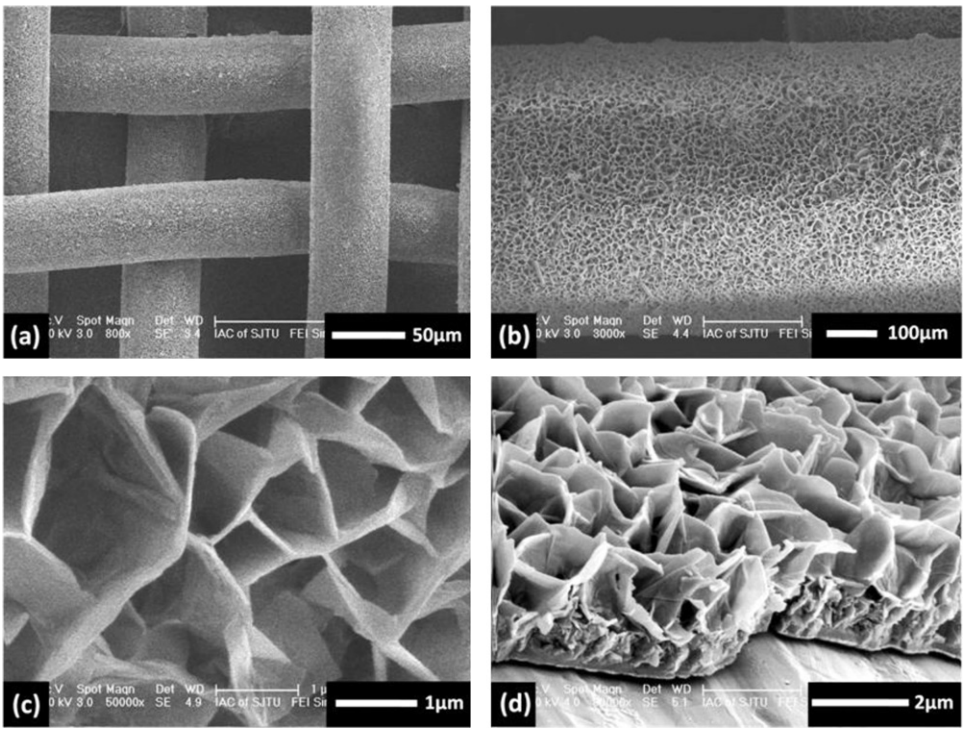

Fig. 1. SEM images of the 2D ZnO nanoflakes coated stainless steel mesh. (a) Large-area view of the coated mesh, (b) top images of the 2D ZnO nanoflakes on one stainless steel wire, (c) high magnification of the as-grown ZnO, and (d) the side images of the ZnO nanoflakes with height about 2 μm.

laboratory oven. Then, the mesh was removed from the solutions, washed with deionized water and dried at 80 °C for 1 h. Finally, the sample was immersed into the ethanol solutions of 8 mM SA ($C_{18}H_{36}O_2$) for 10 h, and then dried in the air.

Surface images of the samples were characterized by field emission scanning electron microscope (SEM, Philips Sirion 200). The X-ray diffraction (XRD) experiment was carried out with D/max-2200/PC type diffraction, using Cu Kα radiation. An optical contact-angle meter system (Data Physics Instrument GmbH, Germany) was used to measure contact angle. Liquid droplets of 5 μl were suspended with needle tube and brought in contact with mesh using a computer controlled device.

3. Results and discussion

Fig. 1(a) shows the large-area view of the 2D ZnO nanoflakes on stainless steel mesh through low-temperature hydrothermal route. The pore size of stainless steel is about 75 μm. Typical image of the 2D ZnO nanoflakes on a stainless steel wire is shown in Fig. 1(b). Fig. 1(c) is the high magnification SEM image of the as-grown ZnO nanoflakes. It is found that each nanoflake is about 1.5 μm in width. We can see from Fig. 1(d) that the 2D ZnO nanoflakes are nearly vertical to the mesh, and each nanoflake is about 2 μm in height. Thus, a kind of interesting morphology of 2D ZnO nanoflakes was achieved on the stainless steel mesh substrate. Fig. 2 shows the XRD pattern of 2D ZnO nanoflakes. The ZnO (1 0 0), (0 0 2) and (1 0 1) peaks are observed besides the (1 1 1) and (2 0 0) peaks which come from Al deposited on the mesh, which further indicates that the 2D nanoflakes is polycrystalline wurtzite ZnO.

The following chemical reaction equation will give the formation process of ZnO. It has been proposed from reactions (1) and (2) that HMT can react with water to produce ammonia which in turn to generate OH^- anions. Because Al is an amphoteric metal, it can be dissolved into the solution under alkaline conditions in the presence of amine (from HMT). So more and more OH^- anions will combine with Al^{3+} and Zn^{2+} to form $Al(OH)_4^-$ and $Zn(OH)_4^{2-}$, as shown in reactions (3) and (4), respectively. ZnO cluster are formed by the dehydration reaction (5). It is well-known that supersaturation is a prerequisite for crystal growth in solution. The growth habit of ZnO nanocrystallites is determined by not only the internal structure of ZnO itself, but also the concentration of OH^- [19]. In general, the wurtzite ZnO crystal grows preferentially along [0 0 1] direction. Furthermore, the additive ions usually act as a regulator to promote or inhibit the growth by their capping on the ZnO surface [20]. $Al(OH)_4^-$ would presumably bind to the Zn^{2+} terminated (0 0 1) surface and suppressed the growth along [0 0 1] direction [21]. Therefore, the ZnO sample shows the morphology of 2D nanoflakes, as shown in

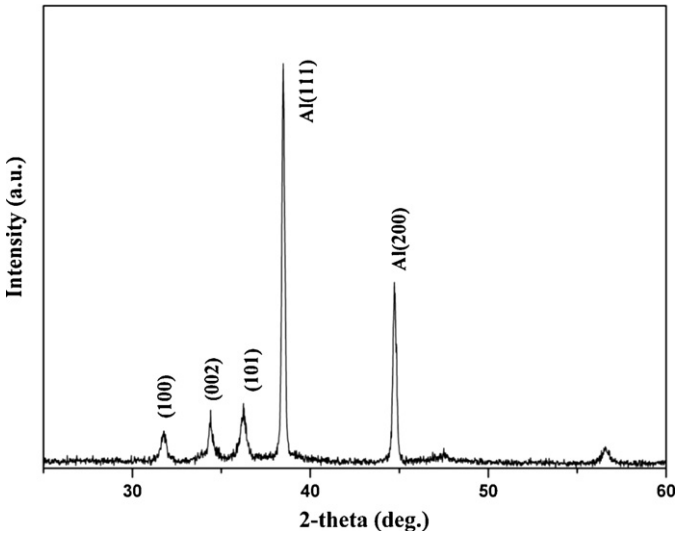

Fig. 2. XRD patterns of the as-grown ZnO sample.

Fig. 1.

$$C_6H_{12}N_6 + H_2O \rightarrow 6HCHO + 4NH_3 \quad (1)$$

$$NH_3 + H_2O \leftrightarrow NH_4^+ + OH^- \quad (2)$$

$$Al^{3+} + 4OH^- \leftrightarrow Al(OH)_4^- \quad (3)$$

$$Zn^{2+} + 2OH^- + 2H_2O \leftrightarrow Zn(OH)_4^{2-} + 2H^+ \quad (4)$$

$$Zn(OH)_4^{2-} + 2H^+ \leftrightarrow ZnO_{cluster} + 3H_2O \quad (5)$$

Fig. 3 shows the Fourier transform infrared (FTIR) spectrum of the coated mesh which was modified by SA. SA is known as a wax-like saturated fatty acid. SA molecules are absorbed onto 2D ZnO nanoflakes and lower its surface free energy. The interaction is confirmed by FTIR spectrum (Fig. 3). Two sharp peaks at about 2918 cm^{-1} (CH3) and 2850 cm^{-1} (CH2) indicate the existence of long-chain aliphatic groups and successful coating of SA molecules. The characteristic peak of the COOH group at 1713 cm^{-1} disappears, indicating that the dissociative SA in the ZnO nanoflakes is very little. One peak appears at 1539 cm^{-1}, assigning to the antisymmetric carboxylate ion COO^- stretching modes.

The separation principle of water and oil through the coated mesh can be explained by the Cassie equation (6) and Wenzel equation (7) [22,23]:

$$\cos\theta^* = -1 + f_1(1 + \cos\theta) \quad (6)$$

$$\cos\theta^* = r\cos\theta \quad (7)$$

where θ^* is the contact angle of a the rough (hydrophobic) substrate, θ is the contact angle of a native flat surface, f_1 is the fraction of solid in contact with liquid (f_1 is a number smaller than unity), the surface roughness r is defined as the ratio of the actual over the apparent surface area of the substrate (r is a number larger than unity). The value of f_1 diminishes quickly, the contact angle increases according to Eq. (6) due to the rough surface and the low surface free energy. Fig. 4(a) shows the water contact angle (WCA) on this coated mesh is about 156.3 ± 2.1°. According to Eq. (7), the surface oleophilicity can be enhanced by the increase of the surface roughness because original stainless steel mesh is oleophilic material. The oil contact angle (OCA) is close to 0°, as shown in Fig. 4(b), and the penetration through the coated mesh is completed quickly as shown in Fig. 4(c).

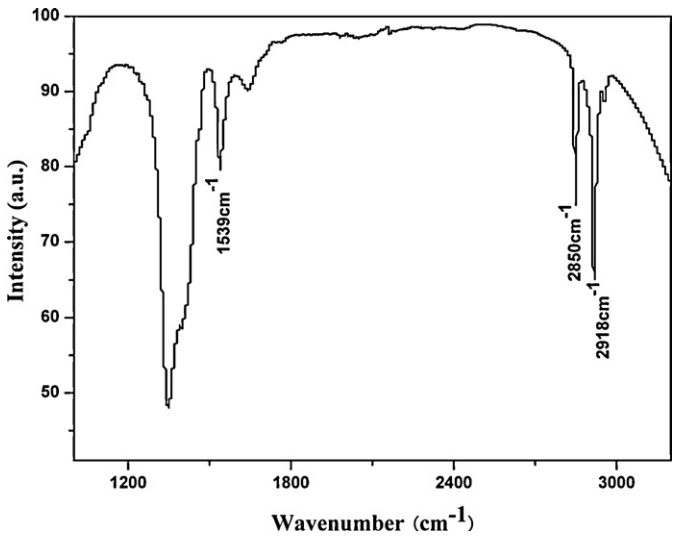

Fig. 3. The Fourier transform infrared spectrum of the SA coated ZnO nanoflakes.

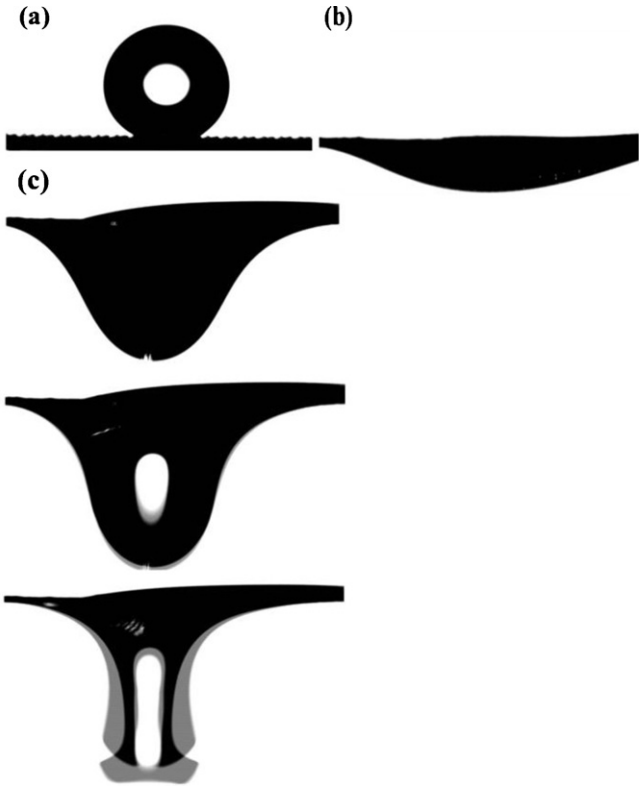

Fig. 4. Shapes of water and oil droplets on the coated mesh. (a) Water contact angle, (b) oil contact angle, and (c) permeating process of diesel oil on the coated mesh.

Fig. 4 indicates the coated mesh can be applied to separate water and oil mixture. The oil was added into deionized water under constant stirring for preparing the mixture of oil and water. As shown in Fig. 5, the mixture of diesel oil and water (30% v/v) was poured onto the mesh, diesel oil quickly permeated through the filter and dropped into the bottle of test tube, meanwhile, water flowed along the outside of test tube into the beaker. In the separation experiments, we used a variety of water and oil mixture, and all the mixture could be successfully separated. The coated mesh retained superhydrophobic and superoleophilic properties after dozens of uses.

It has been reported that the wettability of the mesh depended on the pore size [4,13]. Fig. 6 illustrates the relationship between the contact angles and the pore sizes which range from 25 to 600 μm. From Fig. 6, we can find that the hydrophobicity shows a remarked dependence on pore size while the OCAs are always close to 0°. The coated mesh has optimum superhydrophobicity when the pore diameter of the mesh is about 75 μm. Because of the insufficient proportion of the air/water interface, the mesh is lack of superhydrophobicity when the pore size is below 75 μm. Whereas above 75 μm, the pore size is so large that micro/nanostructured stainless steel thread cannot provide enough hydrophobic force. Hence, a decrease in hydrophobicity is observed when the size of the mesh pore increases further. In our experiments, stainless steel wire with pore size of about 450 μm has a bigger radius than that of 300 μm. Therefore, a stainless steel wire with pore size of about 450 μm has more 2D ZnO nanoflakes which can provide hydrophobic force. This may be the reason why the WCA on the mesh film with pore size of about 300 μm. Therefore, both the special hierarchical micro/nanostructures and the suitable size

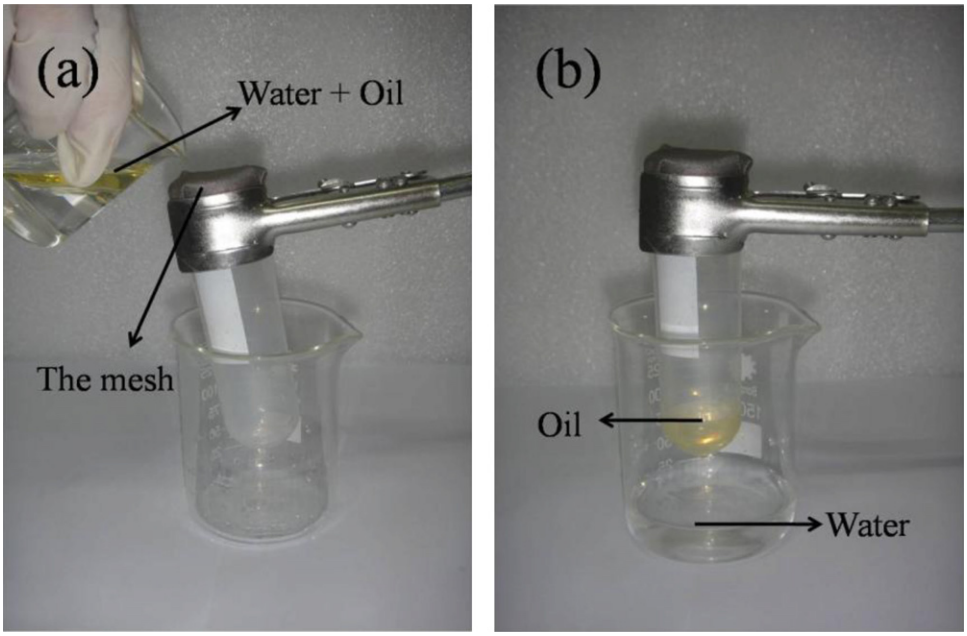

Fig. 5. Experiment process of separation water and oil. (a) Before separation and (b) after separation.

of the mesh pores are important in obtaining the best separation of water and oil.

Many studies have been reported about the separation of water and oil [4,5,8,23], but few results concerned the separation efficiency. In this paper, the separation efficiency was calculated by oil rejection coefficient (R (%)) (8) [24]. In order to get best results, we use the coated mesh with the pore size about 75 μm.

$$R(\%) = \left(1 - \frac{C_p}{C_0}\right) \times 100 \tag{8}$$

where C_0 is the oil concentration of original water and oil mixture and C_p is the oil concentration of collected water after one time separation. We use four kinds of oil in the separation experiments, containing gasoline, diesel, hexane, and petroleum ether. The separation efficiency of diesel and water attains the peak value of 95.3%, as shown in Fig. 7.

To further explore the mechanism that the coated mesh has different separation efficiency for different water and oil mixture, we model the process in Fig. 8 on the assumption that the pores are arranged approximately in a regular square array. It can be shown from Fig. 8 that the position of the three-phase contact line of the meniscus is mainly governed by the differential pressure ΔP [13,25,26]:

$$\Delta P = \frac{2\gamma_{ov}}{R} = -\frac{l\gamma_{ov}(\cos\theta_A)}{A} \tag{9}$$

where γ_{ov} is the surface tension of the oil–vapor interface, R is the meniscus curvature, l is the circumference of the pore, A is the cross-sectional area of the pore, and θ_A is the advancing contact angle of the oil on the surface. It can be seen from Fig. 8(a) and Eq. (9) that $\Delta P > 0$ (negative capillary effect) when $\theta > 90°$, so the coated mesh shows superhydrophobicity. From Fig. 8(a) and Eq. (9), we can see that $\Delta P < 0$ (capillary effect) when $\theta < 90°$, so the coated mesh shows the superoleophilicity. With the increase of the surface tension, the absolute value of the pressure becomes larger, so the oil will penetrate the coated mesh easier. Therefore,

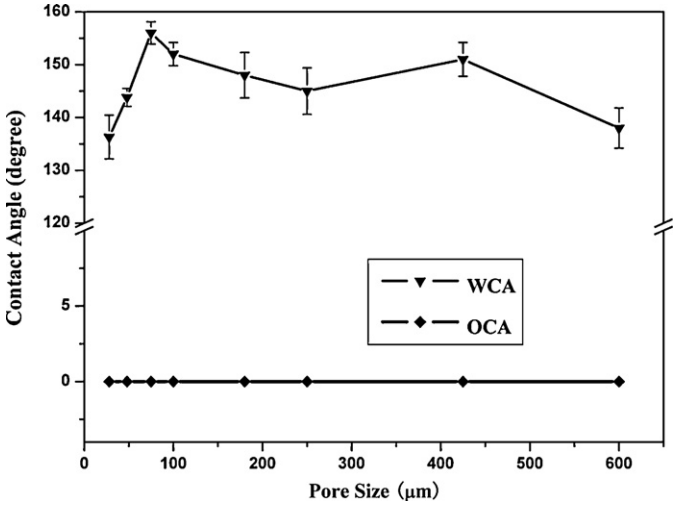

Fig. 6. The relationship between the pore sizes and the contact angles of water and oil on the coated mesh.

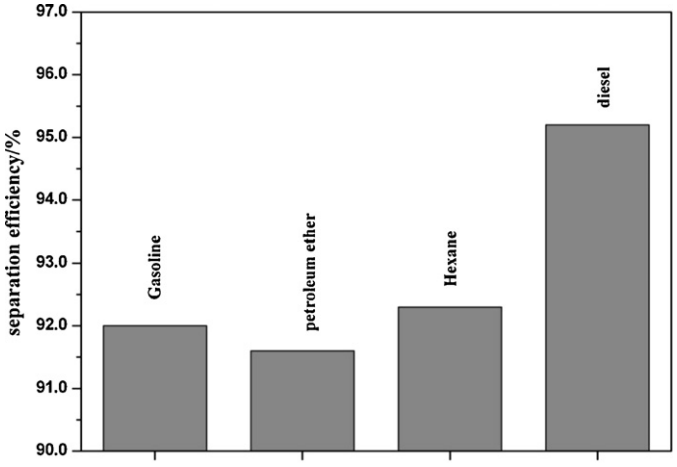

Fig. 7. The separation efficiency of the coated mesh for the different mixture of the water and oil.

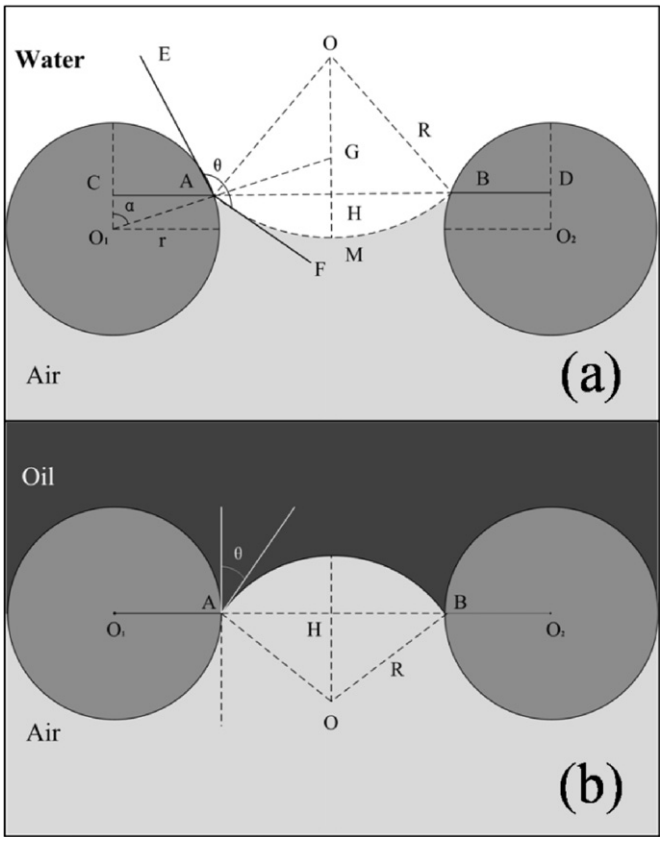

Fig. 8. Schematic diagrams of the wetting model of the mesh film coated by ZnO nanoflakes. (a) Water wetting model of the coated mesh. (b) Oil wetting model of the coated mesh. O is the center of the spherical cap of the meniscus; O_1 and O_2 are the cross-section center of the mesh.

we can infer that the separation efficiency mainly depends on the surface tension. Because $\gamma_{diesel} > \gamma_{hexane} > \gamma_{gaoline} > \gamma_{petroleum\ ether}$, we can draw a conclusion that the separation efficiency is $R_{diesel} > R_{hexane} > R_{gaoline} > R_{petroleum\ ether}$, which is consistent with our experimental results as shown in Fig. 7.

4. Conclusions

In summary, a novel performance of superhydrophobic and superoleophobic 2D ZnO nanoflakes coated mesh was developed through low-temperature hydrothermal route. Because of the special hierarchical micro/nanostructures and appropriate size of the mesh, the coated mesh showed an excellent superhydrophobicity with WCA of about $156.3 \pm 2.1^\circ$ and superoleophobicity with OCA of about 0°. So the coated mesh can be used effectively for the separation of water and oil. In experiment, the coated mesh showed high separation efficiency for a variety of water and oil mixture, which was up to 95%. It was found that the separation efficiency mainly depended on the surface tension of the oil. This work may be expanded to the novel separation and filtration equipment.

Acknowledgements

This work was supported by the Natural Science Foundation of China (grant Nos. 10874115 and 11174197), National Major Basic Research Project of 2012CB934302, and National 863 Program 2011AA050518.

References

[1] S. Hoffmann, W. Nistch, Chem. Eng. Technol. 24 (2001) 22–27.
[2] B. Rosemarie, Chem. Ing. Tech. 58 (1986) 449–456.
[3] J. Yuan, X. Liu, O. Akbulut, J. Hu, S.L. Suib, J. Kong, F. Stellacci, Nat. Nano 32 (2008) 332–336.
[4] L. Feng, Z.Y. Zhang, Z.H. Mai, Y.M. Ma, B.Q. Liu, L. Jiang, D.B. Zhu, Angew. Chem. Int. Ed. 43 (2004) 2012–2014.
[5] T. Sun, L. Feng, X. Gao, L. Jiang, Acc. Chem. Res. 38 (2005) 644–652.
[6] X.J. Feng, L. Jiang, Adv. Mater. 18 (2006) 3063–30688.
[7] H. Gau, S. Herminghaus, P. Lenz, R. Lipowsky, Science 283 (1999) 46–49.
[8] A. Nakajima, A. Fujishima, K. Hashimoto, T. Watanabe, Adv. Mater. 11 (1999) 1365–1368.
[9] S. Herminghaus, Europhys. Lett. 52 (2000) 165–170.
[10] M. Hui, M.J. Blunt, J. Phys. Chem. B 104 (2000) 3833–3845.
[11] K.R. Skull, T.E. Karis, Langmuir 10 (1994) 334–339.
[12] Y. Chen, B. He, J. Lee, N.A. Patankar, J. Colloid Interface Sci. 281 (2005) 458–464.
[13] D.L. Tian, X.F. Zhang, X. Wang, J. Zhai, L. Jiang, Phys. Chem. Chem. Phys. 13 (2011) 14606–14610.
[14] C.H. Lee, N. Johnson, J. Drelich, Y.K. Yap, Carbon 49 (2011) 669–676.
[15] C. Lee, S. Baik, Carbon 48 (2010) 2192–2197.
[16] C.W. Tu, C.H. Tsai, C.F. Wang, S.W. Kuo, F.C. Chang, Macromol. Rapid Commun. 28 (2007) 2262–2266.
[17] Q. Pan, M. Wang, H. Wang, Appl. Surf. Sci. 254 (2008) 6002–6006.
[18] L.J. Yao, M.J. Zheng, C.L. Li, L. Ma, W.Z. Shen, Nanoscale Res. Lett. 7 (2012) 216–223.
[19] B.Q. Cao, W.P. Cai, J. Phys. Chem. C 112 (2008) 680–685.
[20] F. Xu, Z.Y. Yuan, G.H. Du, M. Halasa, B.L. Su, Appl. Phys. A 86 (2007) 181–185.
[21] J.P. Cheng, X.B. Zhang, Z.Q. Luo, Surf. Coat. Technol. 202 (2008) 4681–4686.
[22] A.B.D. Cassie, S. Baxter, Trans. Faraday Soc. 40 (1944) 546–551.
[23] R.N. Wenzel, Lnd. Eng. Chem. 28 (1936) 988–994.
[24] Z.X. Xue, S.T. Wang, L. Lin, L. Chen, M.J. Liu, L. Feng, L. Jiang, Adv. Mater. 23 (2011) 4270–4273.
[25] J.P. Youngblood, T.J. McCarthy, Macromolecules 32 (1999) 6800–6806.
[26] B. Liu, F.F. Lange, J. Colloid Interface Sci. 298 (2006) 899–909.